Journal of Molecular Liquids 268 (2018) 598–609

Contents lists available at ScienceDirect

Journal of Molecular Liquids

journal homepage: www.elsevier.com/locate/molliq

Experimental study of physicochemical changes in water by iterative contact with hydrophilic polymers: A comparison between Cellulose and Nafion

Vittorio Elia [a], Rosario Oliva [a], Elena Napoli [a], Roberto Germano [b,*], Gabriella Pinto [c], Liliana Lista [a], Marcella Niccoli [a], Dario Toso [d], Giuseppe Vitiello [e], Marco Trifuoggi [c], Antonella Giarra [c], Tamar A. Yinnon [f,g]

[a] Department of Chemical Sciences, University "Federico II", Complesso Universitario di Monte Sant'Angelo, Via Cintia, I-80126 Napoli, Italy
[b] PROMETE Srl, CNR Spin off, P.le V. Tecchio, 45, 80125 Napoli, Italy
[c] Analytical Chemistry for Environment Institute of the Chemical Science, Department of the "Federico II" University of Napoli, Italy
[d] DAD - Politecnico di Torino, Viale Mattioli, 39, 10125 Torino, Italy
[e] Department of Physics "E.R. Caianiello", University of Salerno and INFN, Sezione di Napoli, Italy
[f] K. Kalia, D.N. Kikar Jordan, 90666, Israel
[g] Reedmace Lake, Enot Tsukim Nature Reserve at Kalia, Israel

ARTICLE INFO

Article history:
Received 3 April 2018
Received in revised form 10 July 2018
Accepted 11 July 2018
Available online 17 July 2018

Keywords:
Water
Cellulose
Water perturbed by cellulose
Mirror symmetry breaking
Interfacial water

ABSTRACT

Water kept in contact with cellulose has not been a "juicy" research topic until now. This is surprising because cellulose is a major component of the cell walls in green plants. It is also a common material used in many artificial systems, e.g., filters. In this work, we review some of our experimental results and show that iteratively bringing cellulose (cotton wool) in contact with pure water endows the water with some unforeseen properties. For example, the liquid left over after removing the cellulose is optically active, i.e., mirror symmetry breaking was triggered during temporary contact of bulk water with a natural polymer. (Here and in the following, by "mirror" symmetry we actually mean "chiral" symmetry). Moreover, this leftover liquid fluoresces after irradiation with ultraviolet light. These properties are neither attributable to impurities released by the inert polymer nor to organic- or bio-contaminants, as our state-of-the-art analytical techniques show. These techniques include gel electrophoresis, Matrix-Assisted Laser Desorption/Ionization Time of Flight (MALDI-TOF) and Gas Chromatography both coupled with Mass Spectrometry. Instead, the properties are attributable to stabilization of interfacial water adjacent to hydrophilic membranes. Our findings have implications for processes in water flowing adjacent to cellulose, in particular enantioselective processes. Such processes play critical roles in many biosystems and technologies. Thus, our study indicates that water iteratively brought in contact with cellulose merits intensive research.

1. Introduction

Cellulose is the most abundant organic polymer on Earth [1]. It is a major constituent of the cell walls of green plants. It is an important ingredient in many manufactured materials, e.g., paper, textile and food products. It is biodegradable.

Cellulose is insoluble in water (see Section S1). This fact, likely, leads scientists to assume that it does not affect nearby bulk water. However, our recent carefully controlled experiments have shown that cellulose nitrate filters affect the physicochemical properties of bulk Milli-Q water [2, 3]. For example, they affect the water's electric conductivity, density, heat of mixing with acids and ultraviolet (UV) absorption spectra. To amplify the effects, in the experiments reported in Ref. [2, 3], we iteratively filtered the water. The iterative filtration procedure is detailed in Section S2. In the following, such iteratively filtered water will be denoted by IPW-F (Iteratively Perturbed Water by Filtering). The physicochemical variables of IPW-F are correlated [2, 3]. The correlations indicate that a single cause underlies the peculiar physicochemical properties of the filtered water. For example, the linear correlation between the logarithms of electrical conductivity (χ) and density of the perturbed water reflects the fact that this water has scale-free self-similar fractal properties [4]. We showed that the changes induced by the filtering are not simply attributable to chemical impurities, e.g., compounds released by the filter or the filtering apparatus [2]. Instead, these changes result from formation of dissipative structures [3]. The diameter of the structures may reach hundreds of nanometres (nm) [3].

* Corresponding author.
E-mail address: germano@promete.it (R. Germano).

https://doi.org/10.1016/j.molliq.2018.07.045
0167-7322/

Our analyses hinted that the dissipative structures form adjacent to the hydrophilic filter, and that these are flushed into the filtrate during the filtration process [2, 3]. Hydrophilic membranes, like the cellulose filters which we employed, induce the formation of an interfacial water zone, hundreds of microns wide [5, 6]. In the literature, this zone has been denoted "Exclusion Zone (EZ)".[1] We hypothesized that the violent flux of water in the very narrow pores of the filter ruptures clumps of the EZ.

With the aim of an in depth investigation of the formation process of the structures in IPW-F, we iteratively perturbed water with an inert hydrophilic membrane (Nafion®) [7–12]. We chose a Nafion membrane because its interfacial EZ is known to be broad [5, 13, 14]. Its width may reach 1 mm. We immersed the membrane in Milli-Q water, stirred the liquid, removed and dried the membrane, and then repeated these steps several times over. The water left over after removal of the membrane will be denoted by IPW-N (Iteratively Perturbed Water with Nafion). Our analyses of the main physicochemical properties of IPW-N indicate that its dissipative structures are clumps of ruptured EZ water [12] (see Section S3).

The goal of this study was to elucidate the effects on water resulting from iteratively bringing water in contact with cellulose, in a manner that is omnipresent in nature and in artificial systems. To this goal, we repetitively immersed cotton wool in water. After each immersion, we removed the hydrophilic cotton (HC) and dried it in air. The liquid left over after the last contact, i.e., the last HC immersion in water and its subsequent removal, we denote by IPW-HC (Iteratively Perturbed Water by HC).

This study is the first report of experimental data on IPW-HC. The data include the optical microscopy images of IPW-HC, its circular dichroism, pH, density, χ, heat of mixing with an acid, UV radiation absorption and emission. We also report state-of-the-art analyses data to estimate the quantities of impurities in the IPW-HC samples. We analyzed the samples with Gas Chromatography (GC) and Matrix-Assisted Laser Desorption/Ionization Time of Flight (MALDI-TOF), both coupled with Mass Spectrometry (MS), as well as gel electrophoresis and Ion Chromatography (IC).

To expound the similarities and differences between water perturbed by cellulose and that perturbed by a synthetic membrane, we compared the data on IPW-HC with that on IPW-N. The data on the latter have been reported and analyzed in references [4] and [7–12].

2. Results

2.1. Sample and control characterizations

2.1.1. IPW-HC samples

The IPW-HC preparation procedure is detailed in the "Methods" 5.3.1 section. We characterize IPW-HC samples by their electric conductivity ($\chi_{\text{IPW-HC}}$). This parameter depends on the number of HC immersion-removal cycles, the volume of the treated water, the size of the HC piece and fluctuating environmental conditions. $\chi_{\text{IPW-HC}}$ always increases with the number of cycles. We prepared thousands of IPW-HC samples. For some samples, the differences between their $\chi_{\text{IPW-HC}}$ and the electric conductivity of Milli-Q® water were huge, i.e., nearly four orders of magnitude. The electric conductivity of Milli-Q is about 1–2 μS cm^{-1}.

While the IPW-HC samples are stored, for days or even months, their $\chi_{\text{IPW-HC}}$ incessantly changes. $\chi_{\text{IPW-HC}}$ may first increase and subsequently decrease, first decrease and then increase, continuously increase or decrease (see Fig. S1). We have observed similar phenomena for IPW-N and IPW-F (8, 12, 15). These phenomena are typical of far-from-equilibrium, self-organizing and dissipative systems. The values of the experimental variables of these systems depend on the ambient conditions and on the volume of the samples (see Fig. S1). The concentration of impurities cannot increase, decrease and re-increase and so on. Therefore, the storage-time dependence of $\chi_{\text{IPW-HC}}$ is an indirect and clear proof that the naive hypothesis of the presence of impurities underlying the $\chi_{\text{IPW-HC}}$ phenomena is incorrect!

The fact that IPW-HC exhibits qualities typical of far-from-equilibrium, self-organizing, dissipative systems implies that it is impossible to prepare samples with equivalent $\chi_{\text{IPW-HC}}$ values. The same is true for its other physicochemical variables, e.g., pH or density (see Fig. S2 and Fig. S3). In addition, these qualities imply that the measuring techniques affect the physicochemical properties of the samples. The effects of the measuring technique are inconsequential for revealing the typical physicochemical phenomena of this liquid, because the values of the various physicochemical variables are correlated. For example, a linear correlation exists between the logarithm of $\chi_{\text{IPW-HC}}$ and the pH of IPW-HC (see Fig. S2). Moreover, the logarithm of $\chi_{\text{IPW-HC}}$ is linearly correlated with the logarithm of the difference between the density of IPW-HC ($\rho_{\text{IPW-HC}}$) and the density of the Milli-Q water (ρ_{water}), with which the IPW-HC was prepared (see Fig. S3). The density difference is significantly larger than zero, for all samples. The difference resembles that of an aqueous electrolyte solution [16]. *The correlations between widely varying variables like conductivity and density indicate that a single cause underlies the phenomena of IPW-HC* [11]. The aforementioned correlations reflect scale-free self-similar fractal properties of a liquid, e.g., IPW-N or IPW-F, as our mathematical analyses have shown [4].[2] Thus, due to its qualities, IPW-HC exhibits phenomena that are repeatable but not quantitatively reproducible.

IPW-HC being a self-organizing, dissipative system hinders measuring a variety of physicochemical variables for a sample with a definite $\chi_{\text{IPW-HC}}$. Carrying out widely different experiments requires many days. Moreover, it may imply varying laboratory facilities. The $\chi_{\text{IPW-HC}}$ of the sample changes during such measurements periods and shifting ambient conditions. Therefore, to reveal characteristics of IPW-HC, we report physicochemical variables for a few samples with different $\chi_{\text{IPW-HC}}$.

The typical $\chi_{\text{IPW-HC}}$ and other physicochemical phenomena of IPW-HC, which we report in the following, are obtainable by preparing samples with virgin pieces of HC or reusing the same piece for several months. Reusing the HC does not significantly affect the numerical values of the physicochemical properties.

2.1.2. Controls

The Milli-Q water, with which we prepare IPW-HC, we use as a control. As mentioned in Section 1, cellulose is insoluble in water. Therefore, IPW-HC's preparation procedure of temporarily bringing HC in contact with Milli-Q water does not alter the liquid's chemical composition. Accordingly, measurable differences between IPW-HC and Milli-Q water have to be of physical (structural and/or dynamical) origin.

An additional control is IPW-N. During the laborious preparation procedure of IPW-HC, which may span days, impurities may enter the liquid. Most aspects of IPW-HC's preparation procedure, i.e., the repetitive manual immersion of a membrane in Milli-Q water, its removal and drying cycles, are very similar to those used for preparing IPW-N. The sole difference between the procedures is that HC is gently squeezed,

[1] In our discussion in this paper, we refer to the studies and experimental observations on EZ water by G. H. Pollack and his group. Ref. [5a] is the group's first report on EZ water. We thank the anonymous referee for mentioning to us previously studied EZ phenomena in non-Gibbs layer, explained by the general theory of Van der Waals and used for explanation, as an example of periodic colloid structures.

[2] We thank the anonymous referee for noticing that fractal structures are known to appear in binary system aggregations and also in frosty patterns of ordinary water on glass, which shows that water can indeed exhibit molecular fractal organization under appropriate boundary conditions. Our observations with IPW-HC shed light on an additional example of a fractal structure in water and on a possible way to understand its formation. Far from being a trivial observation, molecular self-similarity in water in a number of different physicochemical conditions appears to signal a rich underlying dynamics. As discussed in Section S6, a possible theoretical frame is related to the isomorphism of fractal self-similarity to the coherent state dynamics (see also Ref. [4] and references therein).

while the water in the Petri dish employed for preparing IPW-N is manually gently stirred. Therefore, the extensive experimental data on IPW-N reported in our previous papers constitute reasonable controls.

Other controls are Milli-Q waters perturbed by iterative immersion of Whatman cellulose acetate membranes or cellophane sheets. The data on these systems are concisely summarized in Section 2.8. More details will be published in a different publication.

2.2. Impurity analyses of IPW-HC

To test whether impurities underlie the physicochemical properties of IPW-HC, we employed state-of-the-art analytical techniques. We performed mass spectral (MS) analyses with two different ionization techniques: Matrix-Assisted Laser Desorption/Ionization Time of Flight (MALDI-TOF) and Gas Chromatography (GC), both coupled to electron impact ionization. The limit of detection for MALDI-TOF is around 0.1 pmol/μl, while that for GC is about 5 times higher. The MS analyses performed on different samples rule out signals attributable to organic or biological contaminants (see Fig. S4). To investigate the presence of biological species, which escape MS analyses due to problems in ionization efficiency, we submitted the samples to gel electrophoresis fractionation under denaturing conditions. The gel was then stained by using Coomassie blue dye, resulting in the absence of any colored band corresponding to biological polymers such as proteins (see Fig. S4). The limit of detection of Coomassie stain (GelCode Blue Stain Reagent, Product # 24592) used for gel staining is 0.25 ng/band. Our Ion Chromatography (IC) analyses show that inorganic ions do not underlie the high $\chi_{IPW\text{-}HC}$ values. The prevalence of ionic impurities or ions released by the HC is below the quantification limit. The limit of detection of our IC analyses is of the order of 10^{-1} mg/g. For example, for Cl^- ions it is 0.1 mg/g, for F^- ions it is 0.02 mg/g and for SO_4^- ions it is 0.1 mg/g. Thus our state-of-the-art analytical measurements show that IPW-HC neither contains impurities released by the inert polymer nor organic- or bio-contaminants from the surroundings, at levels above the detection limits. Additional arguments against such impurities or contaminants underlying the IPW-HC phenomena reported below are presented in Section S4.

2.3. Structural analyses of IPW-HC

Fig. 1a presents an optical microscopy image of IPW-HC, wherein we dispersed 1 μm (μm) sized Polystyrene microspheres by Polybead Inc. Aggregates with sizes up to hundreds of microns are observable. Fig. 1b displays an optical microscopy image zoomed on an aggregate. Fig. 1c presents an enlarged image of the aggregate.

For controls, we studied IPW-HC to which we added a Nafion 117 membrane and the polystyrene microspheres, and we also studied Milli-Q water to which we added a Nafion 117 membrane and the polystyrene microspheres. Fig. 1d and e, respectively, present the optical microscopy images of these systems. These figures for example help to determine whether the aggregates in IPW-HC are pieces of HC. Fig. 1e shows that a zone devoid of microspheres exists adjacent to the membrane. Such an interfacial EZ water zone, which exists adjacently to Nafion and other hydrophilic membranes, has been extensively analyzed [12–14, 17]. The zone excludes particles such as: medium sized molecules (dyes, acid-base indicators), large molecules (proteins), bacteria, positively or negatively charged colloidal microspheres with diameters of 0.5–2.0 μm. Accordingly the zone has been designated "Exclusion Zone" (EZ). The zone is also visible in Fig. 1d. Adjacent to the zone, a big aggregate is visible. To its right a smaller aggregate, which is located within the zone, is discernible. Fig. 1f shows an enlarged image of an aggregate located within the zone, bordering on the Nafion. Since the zone excludes large molecules, the presence of aggregates within the zone suggests that they are not composed of HC.

Fig. 1a–c reveal that the aggregate consists of domains, containing smaller domains, which in turn contain even smaller domains, etc., i.e., a typical characteristic of a fractal structure. These figures provide a visual sign that the aggregates present in iteratively perturbed waters

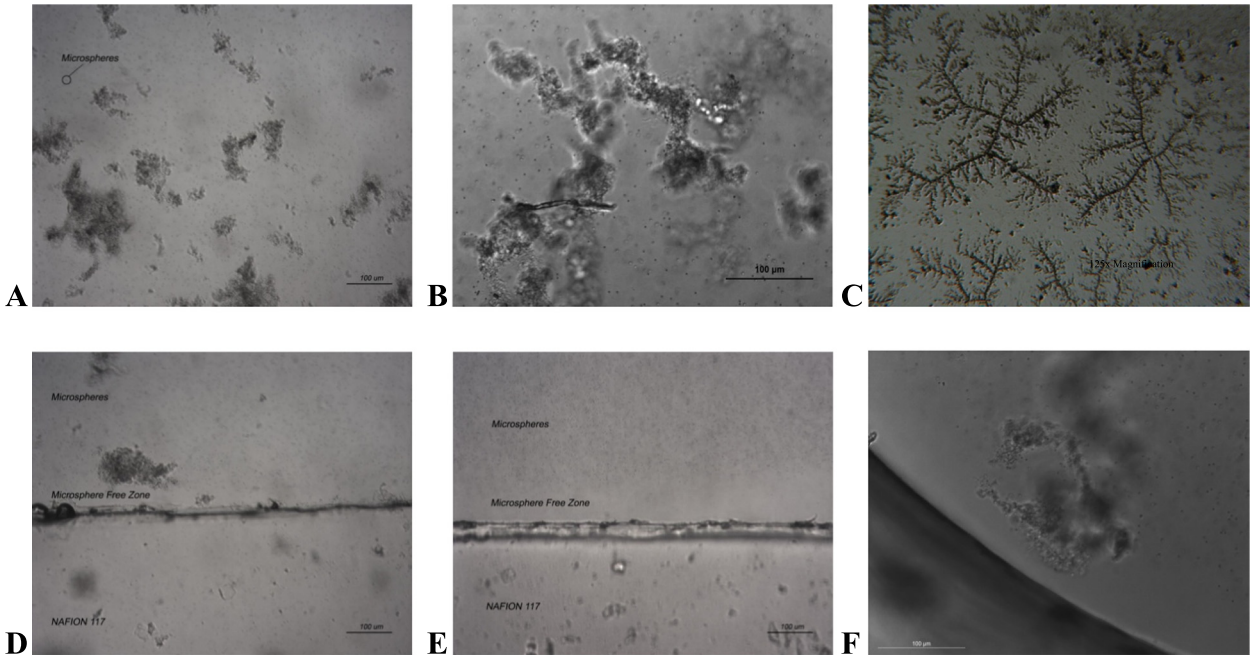

Fig. 1. Optical microscopy images. A. Image of IPW-HC with dispersed 1 μm sized polystyrene microspheres by Polybead Inc. Hundreds-of-microns sized, irregularly shaped aggregates are observable. The tiny spots are the microspheres. B. A magnified image of an aggregate. The image shows that the aggregate consists of domains, containing smaller domains, which in turn contain even smaller domains, etc. C. A 125-time magnified image of an aggregate. The image reveals the scale-free self-similar fractal structure of the aggregate. D. An image of IPW-HC containing a Nafion 117 membrane and 1 μm sized polystyrene microspheres (by Polybead Inc.). A microsphere-free zone adjacent to the membrane is observable. A relatively small aggregate is located within the zone. To its left, just outside the zone, a much larger aggregate is discernible. E. An image of Milli-Q water containing a Nafion 117 membrane and 1 μm sized polystyrene microspheres (by Polybead Inc.). A microsphere-free zone adjacent to the membrane is observable. F. A magnified image of an aggregate located adjacently to the membrane.

containing Polystyrene microspheres have a fractal texture. Evidencing scale-free self-similar fractal properties of a material requires careful mathematical analyses. As mentioned in Section 2.1.1, in Ref. [4] we carried out mathematical analyses that show that the linear correlations between the logarithmic values of widely varying physicochemical variables of perturbed waters, e.g., IPW-N or IPW-F, show these liquids' fractal structure. In Section 2.1.1, we reported the linear correlation between the logarithm of $\chi_{IPW\text{-}HC}$ and the pH of IPW-HC, as well as the linear correlation between the logarithm of $\chi_{IPW\text{-}HC}$ and the logarithm of $(\rho_{IPW\text{-}HC} - \rho_{water})$. According to the analyses carried out in Ref. [4], these correlations show that IPW-HC also has a self similar fractal structure. Hence, the texture visualized in Fig. 1a–c at least is attributable to the fractal quality of IPW-HC. Yet, it is beyond the scope of this paper, to investigate whether the texture of the aggregates in Fig. 1 is solely attributable to the aggregates in IPW-HC. It is possible that the microspheres also contribute to the texture.

The aggregates in IPW-HC, besides their fractal structure and sizes, have other features in common with those observed in IPW-N, as we will show in the following sections. During the IPW-N preparation procedure, on immersing a Nafion membrane in pure water, an interfacial EZ forms. The subsequent stirring of the liquid ruptures the EZ and disperses the resulting clumps in the neighboring bulk water [11, 12]. We can explain the presence of aggregates in IPW-HC in a similar manner. Clumps of interfacial EZ water, which formed adjacently to the HC fibers, are dispersed into the bulk liquid when the HC is squeezed.

2.4. UV absorbance by IPW-HC

The UV absorbance by IPW-HC resembles that of other structured waters. For example, it resembles that of IPW-N, IPW-F, the EZ interfacial water adjacent to Nafion or other hydrophilic membranes and aqueous solutions [3, 5, 7, 18, 19]. Recently, for aqueous solutions, dynamic light scattering in combination with other analyses revealed molecules that were ordered in sub-micron sized aggregates [20]. For instance, such aggregates were observed in sodium chloride solutions with concentrations in the range of 10^{-13} M to 10^{-7} M [20]. IPW-HC, just as the aforementioned structured waters, absorbs in the 200–350 nm wavelength range (see Fig. S5). Conversely, H_2O in the gas phase, bulk water at ambient conditions, amorphous, hexagonal or cubic ice do not significantly absorb radiation in this range [17, 21, 22]. Accordingly, the absorbance in the 200–350 nm wavelength range has been attributed to aggregates composed of H_2O present in structured waters [17, 23]. This is consistent with the predictions of high-level computations: the well-established quantum mechanical ab initio derived Complete-Active-Space Self-Consistent-Field Second-order Perturbation Theory (CASPT2) [23].

2.5. Circular Dichroism (CD) of IPW-HC

Fig. 2 presents the main results of our CD measurements. The figure depicts the CD spectra of various IPW-HC samples. The spectra show the difference between the absorbance of left- and right-handed circularly polarized light as a function of the UV radiation wavelength. The difference [the Delta Absorbance (ΔA) in milli-degrees (mdeg)] is normalized for optical length quartz cuvette (0.5 cm). The temperature (T) of the samples was 20 °C.

Fig. 2 shows that ΔA differs from zero at wavelengths in the 200–240 nm range. ΔA maxima and ΔA minima are located at wavelengths of about 200 nm and 215–222 nm, respectively. The sizeable ΔA values reflect the fact that IPW-HC is optically active. The optical activity implies that perturbing Milli-Q water, by iteratively bringing it in contact with HC, leads to mirror-symmetry breaking The CD spectra of IPW-HC resemble those of β-sheets [24].

Fig. 2a shows that ΔA diminished when the sample was twofold diluted. Fig. 2a and b depict the spectra for IPW-HC samples with different $\chi_{IPW\text{-}HC}$ values, namely 860 and 490 μS cm^{-1}. The figures, as well as our other extensive measurements of ΔA for IPW-HC samples with different $\chi_{IPW\text{-}HC}$, show that ΔA is smaller when $\chi_{IPW\text{-}HC}$ is lower. Fig. 2a also contains the CD spectrum of the control Milli-Q water with χ in the range of 1–2 μS cm^{-1}. The spectrum is flat, because pure water is not optically active – H_2O is achiral. The ΔA phenomena are consistent with IPW-HC containing chiral aggregates, with one type of enantiomer in excess, or only one type being present (homochirality).

The above-mentioned CD spectral features of IPW-HC resemble those of IPW-N [11]. The resemblance suggests that the chiral molecular aggregates in IPW-HC are clumps of interfacial EZ water, dispersed in IPW-HC during its preparation procedure. A hypothesis for the chirality of the aggregates in IPW-N is that chiral conformations evolve during the slow liquid-liquid transition induced by the Nafion membrane in its interfacial EZ water [11]. Most physisorbed achiral molecules order chirally [25]. Such local molecular chirality often gets propagated to the supramolecular level. A similar hypothesis is possible for the chirality of the aggregates in IPW-HC.[3]

We observe a significant difference between the CD of IPW-HC and that of IPW-N after heating. The CD spectra of IPW-HC samples, after these were kept at $T = 90$ °C for 12 or 72 h (h) and subsequently cooled to 20 °C, are presented in Fig. 2b. The figure shows that heating diminishes the ΔA of IPW-HC. However, at most wavelengths in the 200–240 nm range, the ΔA of IPW-HC does not approach zero. In contrast, after keeping IPW-N for prolonged times at $T = 90$ °C, its ΔA approaches zero at these wavelengths [11]. This difference might be due to the composition of the aggregates in IPW-HC compared to the composition of the aggregates in IPW-N. It must be underlined that IPW-N is strongly acidic while IPW-HC is alkaline, as will be detailed further on. The observed decrease in ΔA values of heated samples, compared to the ΔA values of IPW-HC samples that were not heated, is likely due to the chirality of the clumps of EZ water being disrupted by the heat.

The chirality of the aggregates present in IPW-HC, just as that of the aggregates in IPW-N, is not attributable to hydrogen bonding of their H_2O. We added sodium hydroxide (NaOH) or hydrogen chloride (HCl) to IPW-N in amounts sufficient to induce their pH to increase to 13 or to decrease to 3, respectively. The addition of these substances did not disrupt their CD [11]. The same holds for adding high concentrations of Guanidinium chloride to IPW-HC. Our findings imply that interactions, which are much stronger than hydrogen bonds, underlie the secondary structure of the aggregates in IPW-HC or IPW-N. We have started to investigate this surprising phenomenon. Our experiments, however, have not yet clarified this phenomenon.

2.6. Ultraviolet visible (UV–Vis) fluorescence of IPW-HC

Fig. 3 presents fluorescence spectra of IPW-HC samples excited with 280 nm wavelength radiation. We kept the samples at 25 °C. The bandwidths of the excitation and emission monochromator, respectively, were 3 nm and 5 nm. Fig. 3a shows that the spectra consist of two broad overlapping bands. Their widths span wavelengths from about 300 to 500 nm. The maxima of the bands are near 350 nm and 440 nm. We will refer to the band with maximum near 350 nm as the "350 nm band". The band with maximum near 440 nm will be denoted by "440 nm band".

Fig. 3a shows that the 350 nm and the 440 nm bands are absent in Milli-Q water. The emission spectrum of Milli-Q water only contains a very tiny peak at 310 nm. This peak is attributable to Raman scattering

[3] Recently, a chiral water superstructure under near physiological conditions, templated by a deoxyribonucleic acid (DNA) molecule, has been observed [26]. Previously, to differentiate the bulk water response from that of the hydration waters adjacent to DNA, experimentalists relied on cryogenic temperatures, indirect probes, dehydrated DNA, or other methods that likely disrupt the biologically relevant equilibrium hydration. The experimental findings reported in Ref. [26] validate the significance for DNA of our CD results on IPW-HC and IPW-N [27]. To the best of our knowledge, there are no explanations for the findings of Ref. [26].

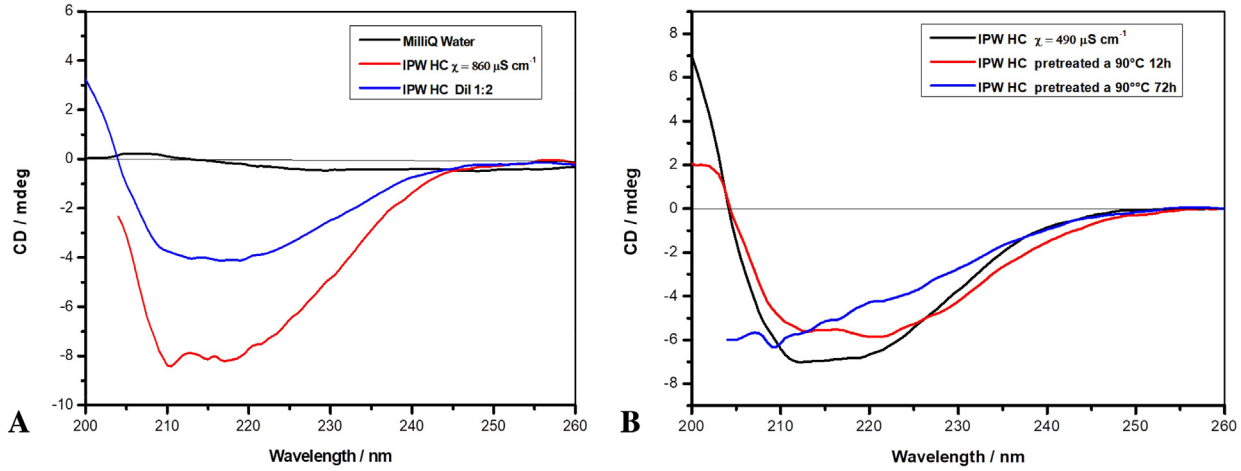

Fig. 2. CD spectra of IPW-HC. The specifications of the samples are noted in the insets. The figure shows that IPW-HC is optically active. It also shows that a twofold dilution of an IPW-HC sample leads to an about twofold reduction of Δ*A*. The figure shows that heating an IPW-HC sample for 12 or 72 h at 90 °C, and subsequently cooling it, affects its Δ*A*.

by H_2O [28]. A tiny peak (shoulder) at 310 nm, resulting from such Raman scattering, is also visible in the fluorescence spectra of the various IPW-HC samples presented in Fig. 3a–d. Even though, for samples with high fluorescence intensities, the Raman peak is rather blurred.

Fig. 3b illustrates that after a twofold or fourfold dilution of the sample, the fluorescence intensity diminishes. Fig. 3c contains the spectrum of a sample heated for 12 or 72 h at 90 °C and subsequently cooled to 25 °C. It shows that the intensity of the 350 nm band strongly diminishes while that of the 440 nm band persists. Fig. 3d shows the effects of filtering a sample. We employed Syringe filters by Corning®, with 200 nm or 450 nm sized pores. The filtering diminishes the intensity of the 350 nm band.

The findings in Fig. 3a and b indicate that the aggregates present in IPW-HC underlie its fluorescence. Dilution reduces their concentration. Fig. 3c hints at two different types of chromophores being present in IPW-HC. One type underlies the 350 nm band. It disappears after prolonged heating of the samples. A second type underlies the 440 nm band. It persists after prolonged heating of the samples. Within this context, we remind that prolonged heating does not eliminate the CD of IPW-HC (see Fig. 2b). Fig. 3d shows that filtering diminishes the intensity of the 350 nm band. The diminishment suggests that filtering eliminates the larger aggregates in IPW-HC underlying the 350 nm band.

The absence of any sharp emission peaks and the smeared out character of the fluorescence spectra of IPW-HC indicate the presence of excimers (see Section S5). Excimers seemingly underlie the structure of the interfacial EZ water adjacent to Nafion and other hydrophilic membranes [17, 23]. The excimers have been studied with the high-level CASPT2 computations. They indicate that EZ water adjacent to hydrophilic membranes contains aggregates that are composed of excimers forming networks of multilayer honeycomb ice-like layers (see Figs. 1 and 6 in Ref. [23]). For example, for the interfacial water adjacent to Nafion, the formula of the excimers is $H_{38}O_{20}$. The formula of the two monomers constituting the excimer is $H_{19}O_{10}$. The H_2O molecules forming the monomer are composed of two fused hexagons. The attractive interaction between the monomers is due to π stacking. In the $H_{38}O_{20}$ networks, the π-stacked H_2O resonate between their ground and an excited electronic state. About 10% of the H_2O constituting the network are simultaneously electronically excited. These results of the CASPT2 model are consistent with those obtained with other models (11), which are presented in Refs. [29] and [30].

The significant interaction between IPW-HC and light is not just apparent from the above reported spectral measurements. It is noticeable with the naked eye. IPW-HC has a yellowish-brownish color. The same is true for IPW-N. The color becomes more clear-cut when, during the preparation of these liquids, their electric conductivity increases.

2.7. Titration phenomena of IPW-HC

Fig. 4a–c present, respectively, the results of pH-metric, conductometric and calorimetric titrations of three IPW-HC samples. Tables S1 and S2 present the numerical values displayed in Fig. 4. The titrations were carried out with HCl or NaOH. The electric conductivity ($\chi_{IPW\text{-}HC}$) of the three samples prior to their titration differed. Their initial conductivities were, respectively, 238 μS cm^{-1}, 358 μS cm^{-1} and 470 μS cm^{-1}. The main titration features of these three samples are similar. These features resemble the ones we observed for many other IPW-HC samples with different initial conductivity.

We performed the pH-metric titrations by measuring the pH of a solution of IPW-HC (1–3 mL) as a function of the volume of added HCl. In other words, we measured the pH as a function of the concentration (mol L^{-1}) of HCl in the final solution. This concentration we denote by M^f_{HCl}. We carried out the conductometric titrations by measuring the electrical conductivity χ as a function of M^f_{HCl}. The procedure for calorimetric titrations involves measuring the mixing heat ΔH_{mix} (see Method Section 5.3.13). We obtained ΔH_{mix} by mixing an IPW-HC sample with increasing amounts of NaOH. The molality of NaOH in the final mixture we denote by m^f_{NaOH} (=mol kg^{-1}). The heat of mixing of IPW-HC with HCl is very low compared to the heat of mixing of IPW-HC with NaOH. It is too low to enable receiving significant titration patterns.

Fig. 4a shows that IPW-HC is alkaline. Fig. 4a and b show that the features of the pH-metric and conductometric titrations of IPW-HC resemble those of titrations of a weak base with a strong acid. A kind of smeared out breakpoint is noticeable in Fig. 4a. It indicates that IPW-HC is a weak base with a dissociation constant of about 10^{-5} mol L^{-1}. A kind of equivalent point is discernible in Fig. 4b. The pH-metric titrations reveal that IPW-HC contains entities that reduce the activity of the hydronium ions (H_3O^+) of the added acid. The conductometric titrations reveal that the entities present in IPW-HC reduce the mobility and/or concentration of the added H_3O^+. The calorimetric titration curve has the shape of a rectangular hyperbola ending in a plateau. This shape typifies formation of an association complex [31]. As such, the calorimetric titration curve reveals some kind of interactions between hydroxyl ions (OH^-) and entities in IPW-HC.

The simplistic explanation that the titration phenomena are due to electrolytic impurities is easy to reject (see Section S4). Instead, the phenomena are explainable within the context of our model of IPW-HC. We

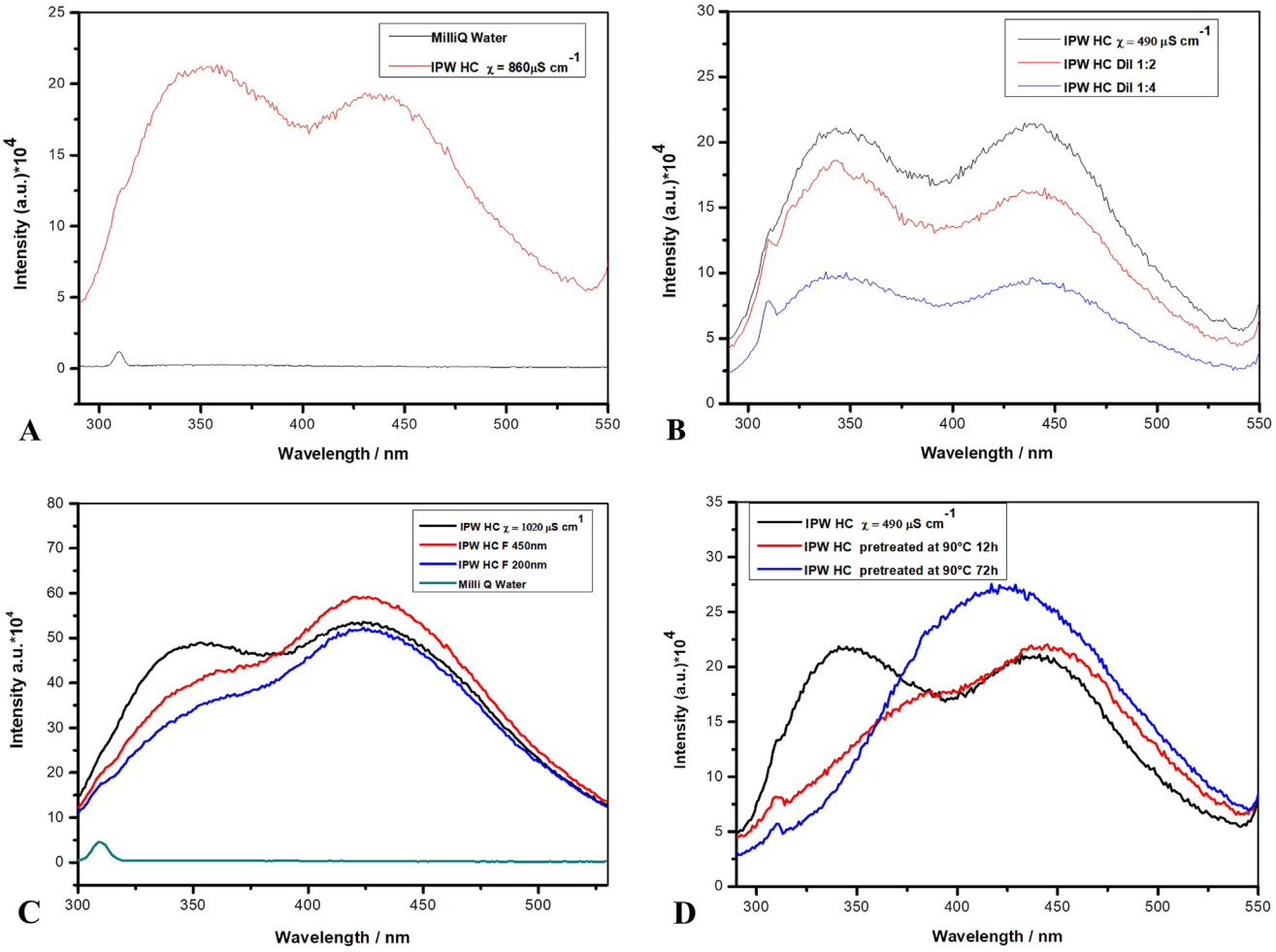

Fig. 3. Fluorescence spectra of IPW-HC. The specifications of the samples are noted in the insets. The fluorescence intensity is presented in arbitrary units (a.u.) (cf. comments at the end of Section 5.3.12). The fluorescence spectrum of IPW-HC has two broad peaks. The peak in the spectrum of Milli-Q water is due to Raman scattering. The denotations Dil 1:2 and Dil 1:4 indicate that the samples were, respectively, twofold and fourfold diluted. The figure shows that dilution reduces the intensity of the fluorescence. The figure shows that heating an IPW-HC sample for 12 or 72 h at 90 °C, and subsequently cooling it, affects its spectral features. The denotations F 450 μm and F 200 μm indicate that IPW-HC samples were filtered with filters which had pore sizes of, respectively, 450 μm and 200 μm.

conjecture that the alkalinity of IPW-HC is due to the presence of its aggregates, i.e., its dispersed clumps of ruptured interfacial EZ water. Specifically, we conjecture that HC shifts the dissociation constant of H_2O in its interfacial EZ water. The H_3O^+ ions stick within the zone and the OH^- ions move to the outer border of the zone. Consequently, IPW-HC consists of positively charged clumps of ruptured interfacial EZ water dispersed in water containing OH^-. In the presence of the aggregates, the dissociation constant of H_2O remains shifted. Our conjecture is inspired by the experimental data on reactive metal sheets, on Nafion and on IPW-N. Reactive metal sheets or Nafion shift the dissociation constant of H_2O in their interfacial EZ water. The interfacial EZ water adjacent to reactive metal sheets is positively charged [32]. The bulk water at the outside border of their interfacial EZ water is alkaline (pH of about 8–9). The interfacial EZ water adjacent to Nafion is negatively charged [33]. The bulk water at the outside border of its interfacial EZ water is acidic (pH of about 3). IPW-N is acidic – its pH may reach values as low as 3 [8]. The effect of HC on the dissociation of H_2O in its interfacial water has not yet been measured.

The titration phenomena are consistent with our conjecture that IPW-HC is composed of positively charged clumps of ruptured interfacial EZ water dispersed in water containing OH^-. The pH-metric and conductometric titration data are explainable by the added H_3O^+ ions neutralizing OH^-, i.e. reducing the concentration of the excess OH^-. The calorimetric titration curve is explainable by the added OH^- ions combining with the positively charged aggregates. As to the driving force underlying the association, our thermodynamic data, summarized in Table S3, indicate that it is essentially of entropic nature. Both the standard molar enthalpy of association and the standard molar entropy are high and negative. For instance, in a sample with $\chi_{IPW\text{-}HC} = 238$ μS cm^{-1}, the standard molar enthalpy of association is -117.0 kJ mol^{-1} and the entropy multiplied by the temperature is -93.1 kJ mol^{-1}. These parameters vary from sample to sample. In contrast, the standard free energy is similar even for samples with very different $\chi_{IPW\text{-}HC}$.

The properties of alkalinity, electric conductivity, calorimetry and titration that characterize IPW-HC are similar to those found for IPW-F [2, 3, 10]. These properties also are similar to those of water perturbed by other methods [34–36]. In-depth explanations of these properties are provided in Ref. [37]. For example, in Section 2.8, 3.1 and 3.2.1 of Ref. [37], electric conductivity phenomena of IPW-F are explained. In particular, these sections focus on the enhancement in the electric conductivity of water when it is perturbed by iterative filtrations. It is beyond the scope of this paper to dwell on the intricate analyses required to explain the impact of perturbations on the physicochemical properties of water. Instead, we just point out that whenever perturbing water stabilizes aggregates of the type mentioned in Section S6, i.e., coherent domains, the electric conductivity may steeply increase [37].

Looking at Fig. 4, the equivalent point of the conductometric titrations reveals the order of magnitude of the aggregates' concentration in IPW-HC. The same holds for the smeared out breakpoints in the

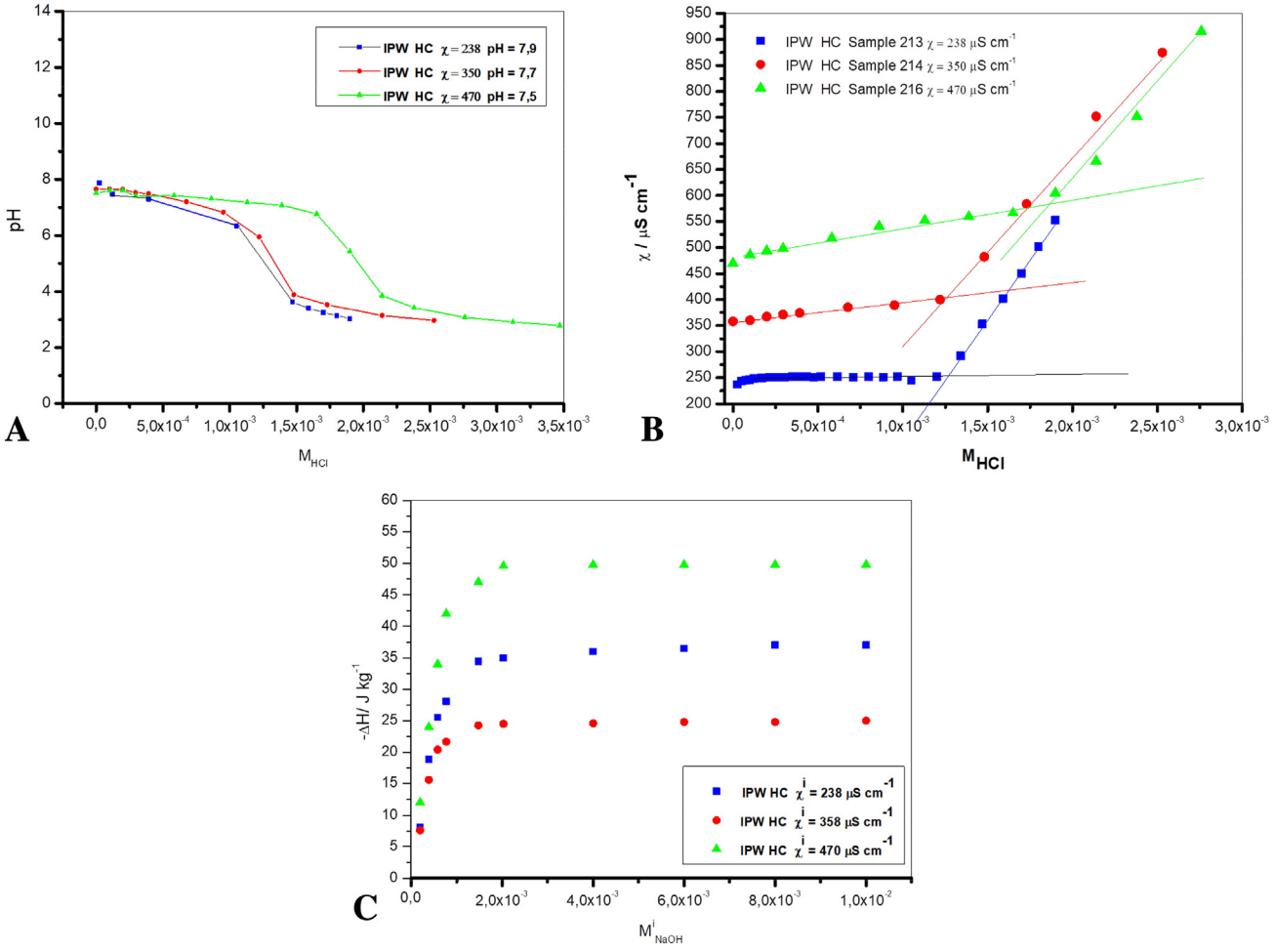

Fig. 4. Titrations of IPW-HC. The pH of three IPW-HC samples titrated with HCl. The initial conductivity and the pH of the samples are given in the inset. The electric conductivity χ of IPW-HC samples titrated with HCl. The initial conductivity of each sample is given in the inset. The heat of mixing ΔH ($=\Delta H_{mix}$ defined in Section 5.3.13) of IPW-HC samples titrated with NaOH. The initial conductivity of each sample is given in the inset.

pH-metric titrations. The concentration is about 10^{-3} mol L^{-1}. It is higher for samples with larger $\chi_{IPW\text{-}HC}$. Thus, the electric conductivity is an indicator of the prevalence of the aggregates.

2.8. IPW-HC compared to other perturbed waters

The iterated contact between water and HC, or Nafion, produces liquids with remarkably similar as well as dissimilar properties. Fig. 5 illustrates some of these properties. Others, which we pointed out in the previous subsections, are summarized in Table S4.

Fig. 5 illustrates that the pH is linearly correlated with the logarithm of the electric conductivity χ for IPW-HC as well as for IPW-N. However, the slopes of the linear functions have opposite signs. Moreover, the magnitudes of the slopes differ. The difference in sign highlights the alkalinity of IPW-HC versus the acidity of IPW-N [8]. The different magnitude is related to the scale-free character of the relations between the pH and log (χ) (see Section S6).

The similarities between the properties of IPW-HC and IPW-N are attributable to their aggregates (the clumps of ruptured interfacial EZ water). The dissimilarities may be due to the nature of the inert HC and the inert Nafion. The surface characteristics of the solid determine the properties of its interfacial water, e.g., its electric conductivity, pH or width [5, 6, 32, 33]. The dissimilarities may also be due to the differences in the perturbation procedure employed for preparing IPW-HC and IPW-N.

Fig. 5 shows that the maximal χ values of IPW-HC samples are about one order of magnitude larger than those of IPW-N. As noted earlier, χ is correlated with the prevalence of the aggregates in these liquid; the maximal concentration of aggregates in IPW-HC is of the order of 10^{-3} mol L^{-1}. This is one order of magnitude higher than that of IPW-

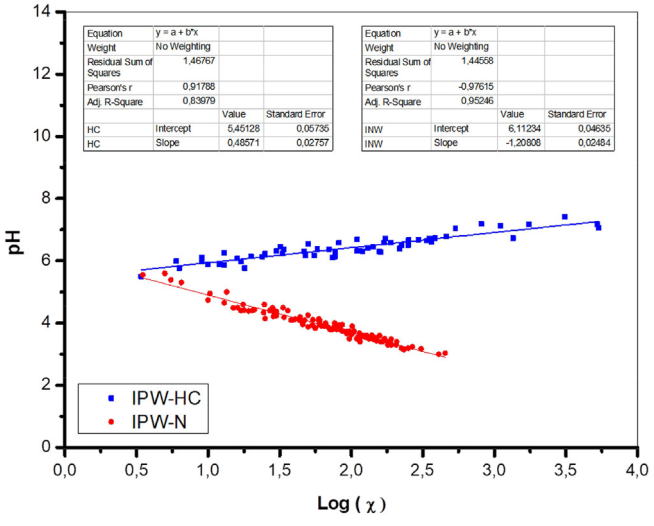

Fig. 5. The pH versus the logarithm of the electric conductivity χ in μS cm^{-1} of IPW-HC and of IPW-N samples. The graph shows that: (a) IPW-HC is alkaline while IPW-N is acid; (b) the maximal χ of IPW-HC is about an order of magnitude higher than that of IPW-N; (c) the pH and log (χ) are linearly correlated.

N (10^{-4} mol L^{-1}) [9]. This dissimilarity may be attributable to the surface area of HC differing from that of Nafion. HC is composed of many strings. Therefore, its surface area is much larger than that of a piece of Nafion membrane. The larger area implies a larger amount of interfacial EZ water. So, perturbing water with HC may produce larger amounts of ruptured EZ water clumps than perturbing it with a Nafion membrane.

We have investigated water perturbed by other types of cellulose, such as Whatman cellulose acetate membranes or cellophane sheets. We perturbed the water in a manner similar to that employed for perturbing water with Nafion. All these perturbed waters are optically active, fluorescent in the UV–Vis range and their pH linearly depends on the logarithm of their χ. This implies that the different hydrophilic groups attached to the D-glucose chains of these cellulose types did not significantly affect the aforementioned physicochemical properties. Details of these properties will be described in a future paper.

3. Discussion and summary

Our measurements on IPW-HC unambiguously show the altered physicochemical properties and structure of water resulting from iteratively bringing it in contact with a natural cellulose polymer (cotton wool). The main results, some implications and examples of still open questions are as follows: The pH-metric and conductometric titrations reveal the presence of entities that reduce the activity, mobility and/or concentration of the H_3O^+ of an added acid. The calorimetric titration curve indicates formation of an association complex.

The order of magnitude of the concentration of the entities in IPW-HC is indicated by the equivalent point of the conductometric titrations and the breakpoint in the pH-metric titrations. The concentration is higher for samples with larger electric conductivity. The conductivity depends on the number of cellulose immersion-removal cycles. After each cycle, it increases, implying that the concentration of the entities increases.

Repetitions of the immersion-removal cycles are required for producing entities in quantities that enable observing their statistically significantly impact on the liquid's physicochemical variables. After about a few hundred cycles (≅200 ÷ 300), the conductivity approaches a maximum, i.e., a value which is about four orders of magnitude larger than the conductivity of Milli-Q water. Currently, we do not have any definite explanation for the appearance of the maximum. Maybe, the maximum indicates that the liquid reaches a saturation.

On storage of IPW-HC samples for days or many months at ambient conditions, their conductivity incessantly changes (see Fig. S1). It may first increase and subsequently decrease, first decrease and then increase, continuously increase or decrease. This phenomenon is typical of far-from-equilibrium, self-organizing and dissipative systems. The phenomenon implies that the naive hypothesis of the presence of impurities underlying the conductivity cannot hold. The concentration of impurities in closed samples does not increase, decrease and re-increase and so on. Instead, the phenomenon indicates that the concentration of the entities changes over time.

The stability of the entities over macroscopic times is intriguing. The stability is similar to that of the entities in IPW-N and IPW-F. For these liquids, attempts to explain the stability are presented in Refs. [10, 12] and [37]. Long range electrodynamic forces seem to play a role.

The UV absorbance and fluorescence spectra of IPW-HC resemble those of "structured waters", such as many types of aqueous solutions [18–20]. During the last decade, aqueous solutions of numerous solutes (alkali chlorides and other strong electrolytes, weak electrolytes and non-electrolytes) have shown to be structured (for a review see Ref. [20]). Dynamic light scattering (DLS) and other techniques have revealed presence of supramolecular domains with sizes in the range of 10^2–10^5 nm for example in solutions with concentrations of 10^{-7}–10^{-13} M and lower. The domains may persist for 1 ÷ 15 months or longer. The domains are not nanobubbles of the gases present in solutions. At concentrations below about 10^{-7} M, the domains mainly consist of H_2O. The UV absorbance intensity of these solutions depends on the prevalence and sizes of the domains observed by DLS [19, 20, 38]. For IPW-HC, experiments employing DLS and other techniques for elucidating the dependence of its UV spectral intensities on its molecular association are warranted.

The optical microscopy images of IPW-HC display the presence of up to 10^5 nm sized aggregates (see Fig. 1). Likely, these are the entities (association complexes) underlying the titration phenomena of IPW-HC, its structuring apparent from its UV spectra and its circular dichroism. However, we cannot exclude that iteratively bringing HC in contact with pure water alters other aspects of the liquid, affecting its spectra and physicochemical properties.

The physicochemical properties of IPW-HC resemble those of waters perturbed by iterative contact with artificial Nafion polymeric membranes, Whatman cellulose acetate membranes or cellophane sheets. The properties also resemble those of waters perturbed by iterative filtering through cellulose nitrate filters. The resemblances indicate that similar processes occur in all of these perturbed waters. Our group extensively analyzed the waters perturbed by Nafion or filtering [2–4, 7–12, 15, 37]. These liquid are far-from-equilibrium dissipative systems. Characteristics of such systems are studied in Refs. [39–48]. The characteristics are consistent with properties of perturbed waters [4, 7, 10, 12, 29, 30, 37, 49, 50]. For IPW-HC, we still have to carry out in depth analyses assessing that all its measured properties conform to those computed by the formulism employed in Refs. [39–48]. Such analyses are outside the scope of this paper. Instead in Section S6, we discuss two aspects of modeling iteratively perturbed waters: symmetry breaking and scale-free self-similar fractality.

The UV spectral and titration data of IPW-HC, IPW-F and IPW-N have many similarities. However, as we pointed out in Section 2, distinctive differences exist. For example, IPW-HC and IPW-F are alkaline, whereas IPW-N is acidic. Currently, we are gathering more data for uncovering similarities and differences not reported in this paper. Moreover, we are widening the kind of materials with which we perturb water, e.g., silk, hemp or clay.

4. Conclusions

Our study overturns the customary assumption that cellulose does not affect nearby bulk water. Our findings are significant for many scientific and technological fields. In numerous natural and artificial systems, water is in contact with cellulose or flows adjacent to it. Such water's dissipative structures have to be considered, for example, when studying reaction dynamics. Such water's physicochemical properties, e.g., its electric conductivity and density being much higher than that of Milli-Q water, may have to be taken into account when investigating chemical or biological processes. The chirality of its aggregates may have major implications. Supramolecular chirality impinges on parts or the whole of multi-component systems (their structure, dynamics and performance). It plays important roles in bioprocesses, nonlinear optics, polymer science, molecular devices, catalysis, materials science, molecular and chiral recognition. Moreover, the mirror-symmetry breaking we observed may have implications for explaining biohomochirality, i.e., why many molecules in natural biosystems have been found to be chiral and to have the same chirality [51]. For example, DNA only contains dextro-rotatory carbohydrates. Biohomochirality has been extensively studied. As to its origin, numerous hypotheses exist [52], including water playing a role [53]; yet this remains enigmatic. Based on our data, we surmise that the chiral aggregates in water perturbed by cellulose may significantly contribute to the origin as well as pervasiveness of biohomochirality. Conceivably, homochiral aggregates form when water very gently or turbulently flows near cellulose. These aggregates may affect the ordering of biomolecules. Thus, our study points to the need for research assessing the effects of cellulose membranes on processes taking place in its nearby bulk water.

5. Materials and methods

5.1. Experimental design

5.1.1. Research objectives

The main objective of our study was to investigate whether water, after iterated contact with cellulose, significantly deviates from Milli-Q water.

5.1.2. Sample size

IPW-HC samples are far-from-equilibrium, self-organizing and dissipative liquids. Therefore, their phenomena are repeatable but not quantitatively reproducible. Consequently, we applied the measuring methods described below to many samples of IPW-HC. Typically, we measured the properties of many tens of samples until we were sure that we discovered a repeatable phenomenon, i.e., a discernible difference between the properties of IPW-HC and those of Milli-Q water.

5.1.3. Analyses

We carried out a number of analyses to determine the chemical composition and purity of IPW-HC, namely: MALDI-TOF/MS, GC/MS, IC and gel electrophoresis fractionation. We analyzed IPW-HC with the following techniques: optical microscopy, measurements of their UV absorption, CD, UV–Vis fluorescence, electric conductivity, pH, density and heat of mixing.

5.2. Materials

We prepared IPW-HC employing commercial HC. The commercial specifications of the HC indicate that it is composed of 100% cellulose. To determine the presence of inorganic molecules in the HC, we incinerated it in an alkaline environment and dissolved the calcined samples in aqueous HNO_3 [see Method Section 5.3.8 Ion Chromatography (IC)]. The resulting solutions we analyzed with IC. The analyses show that the inorganic molecules present in the calcined samples are below the quantification limits.

5.3. Methods

5.3.1. Preparation of water iteratively brought in contact with HC

We washed a piece of HC in Milli-Q® water. Subsequently, we placed the piece in 10–50 mL Milli-Q water (kept in an open polystyrene Petri dish). The size of the piece was about that of the surface of the dish. We let the HC absorb the water. After about 15–30 min, we manually squeezed the HC. Our hands were covered with polyethylene gloves. We squeezed the HC until the majority of its liquid was released into the dish. We dried the HC in air under ambient conditions. Then we took 1 mL of the liquid from the dish and measured its electric conductivity (χ). After about 12 h, we returned the dried piece of HC to the liquid in the dish. We repeated tens of times this cycle of HC immersion, squeezing, drying, taking 1 mL of liquid from the dish and measuring its χ. χ increased after each cycle. The liquid left over after the last HC removal step, we denote by IPW-HC (Iterative Perturbed Water by HC).

5.3.2. Electric conductivity measurements

We systematically performed measurements of the specific conductivity of the samples, using a Radiometer CDM 210 conductivity meter, having a conductivity cell constant of 0.1 cm^{-1}. Before measuring the conductivity of a sample, the cell was calibrated by determining the cell constant K (cm^{-1}). The conductometric titrations were performed in a thermostatic room (25 ± 1 °C), using samples that had been temperature conditioned in a measuring cell by a thermostat-cryostat (Grant LTD6) to within ±0.1 °C.

5.3.3. pH measurements

The pH measurements were carried out with a potentiometer-pH meter (Crison GLP 21–22), having a resolution of ±0.01 pH units. The temperature was controlled within ±0.1 °C with a thermostat-cryostat (Grant LTD6).

5.3.4. Density measurements

We measured the density (g cm^{-3}) of IPW-HC and of Milli-Q water with a vibrating-tube digital density meter (model DMA 5000 by Anton Paar, Austria) with a precision of $\pm 1 \times 10^{-6}$ g cm^{-3} and an accuracy of $\pm 5 \times 10^{-6}$ g cm^{-3}. We controlled the temperature of the water around the densitometer cell to ±0.001 K. We calibrated the densitometer periodically with dry air and pure water.

5.3.5. Gas Chromatography (GC) coupled with Mass Spectrometry (MS)

The GC analyses were performed with an Agilent 6890 Series GC, coupled to a MS 5973 detector. A DB-5ms capillary column (30 m × 0.25 mm ID, 0.25 μm film, 5% phenyl 95% polydimethylsiloxane) was used for the analyses by employing Helium flushed as carrier gas at a flow-rate of 1.0 mL/min. The gradient used for analysis was as follows: 45 °C for 3 min, 150 °C to 12 °C/min, 230 °C to 18 °C/min, 250 °C to 19 °C/min. The analyzer of the GC was maintained at 250 °C. The collision energy in the source was set to 70 eV and the resulting fragment ions were analyzed in the mass range 18–450 *m/z*.

5.3.6. Matrix-assisted laser desorption/ionization time of flight (MALDI-TOF) coupled with MS

MALDI-TOF spectra were acquired by using a 4800 Plus MALDI-TOF mass spectrometer by AB Sciex. Aliquots of samples (1 μL) were directly mixed on the sample-holding plate with an equal volume of 2,5-Dihydroxybenzoic acid matrix dissolved in 70% ACN, 30% formic acid 0.1% (10 mg/mL). The analyses were performed in positive mode, setting the instruments in reflector mode, in the mass range 100–500 *m/z*. Laser power was set to 3500 V for MS spectra acquisition. Each spectrum represents the sum of 3000 laser pulses from randomly chosen spots per sample position. All analyses were performed in triplicate. Raw data were analyzed using Data Explorer Software, version 4.9 (build 115), from Applied Biosystems. The data are reported as monoisotopic masses.

5.3.7. Gel electrophoresis

The samples were loaded on a 12% SDS polyacrylamide gel. The gels were extensively washed in water, stained with Coomassie Blue R-250 and then destained and dried.

5.3.8. Ion Chromatography (IC)

We determined the concentration of inorganic molecules, specifically halide ions, which hypothetically might be present in the commercial cotton wool, by the following processes: We incinerated pieces of wool in an alkaline environment, dissolved the calcined samples in aqueous HNO_3 and investigated the resulting solutions with anionic IC. The details of these processes are: We thoroughly minced a piece of cotton wool weighing 250 mg and subsequently mixed it with 2.5 g of alkaline Eschka (MgO/Na_2CO_3 in 2:1 ratio); we calcined the mixture in a muffle at 600 °C, for 3 h, in a porcelain crucible with a lid; we dissolved the calcined sample in aqueous HNO_3 2 M; the resulting solution we neutralized by adding aqueous NaOH 1 N until its pH was 7; to obtain a 200 mL solution, we added ultrapure water (conductivity <0.06 μS/cm); we investigated the presence of inorganic molecules in the solution with the APAT IRSA CNR 4020 Man 29/2003 IC method. We used a Metrohm IC 883 with conductivity detector, using an A Supp 7 column by Metrosep (250 mm length, 4.0 mm diameter) consisting of a stationary phase of polyvinyl alcohol functionalized by quaternary ammonium groups, with a particle size of 5 μm, and a mobile phase consisting of a solution of sodium carbonate 3.6 mM. We compared the IC results with those obtained by analyzing a “blank”. The “blank” we prepared

according to the same procedures, using the same reagents at the same quantities as those used for preparing the aforementioned solution, with the sole difference that no cotton wool was added. The results show that the measured ions are below the quantification limits.

5.3.9. Optical microscopy

The suspension used for determining the EZ size consisted of 1 μm polystyrene microspheres (by Polysciences Inc.). The microspheres were suspended in deionized water (DI water) obtained from a Barnstead D3750 NANOpure Diamond purification system (type 1 HPLC grade: 18.2 MΩ). The interaction of the microspheres with IPW-HC and IPW-N was observed using an inverted microscope (Leica DM IRB). All image processing was done via LAS V4 software.

5.3.10. UV–Vis spectroscopy

The UV–Vis spectra have been monitored using a Jasco Spectrophotometer, model V-560 UV/Vis. This is a double beam spectrophotometer with double monochromator, a wavelength range of 190–900 nm and a resolution of 0.1 nm. The photometric accuracy and reproducibility of the instrument are, respectively, ±0.002 and ±0.001; the recording conditions for each UV–Vis spectrum were the following: response: slow; scanning speed: 100 nm/min; sampling interval: 1 nm/data. The optical path of the cuvette was 1 cm.

5.3.11. Circular Dichroism spectroscopy

We recorded Far-UV CD spectra using a JASCO J-715 spectropolarimeter (Jasco Corporation, Tokyo, Japan) as the average of 3 scans with 20 nm/min scan speed, 4 s response time, and 2 nm bandwidth, using a 0.1 or 0.5 cm path-length quartz cuvette, at temperature of 25 °C.

5.3.12. UV–Vis fluorescence

The fluorescence spectroscopy measurements were performed by a Fluoromax-4 by Horiba Scientific (Edison, NJ, USA). It is equipped with a Xenon source. The slits on the excitation and emission monochromators have width of, respectively, 3 nm and 5 nm. The samples were loaded in quartz cuvettes with 1 cm path length. After their loading, we enabled a 15 min thermal equilibration. The spectra were recorded at the temperature of 25 °C. As to the successively diluted IPW-HC samples, after each dilution we waited at least 15 min for their thermal equilibration at 25 °C. As customary, the fluorescence intensities are reported in arbitrary units (a.u.). The fluorescence intensity depends on the experimental settings (e.g. optical configuration of the instrument). In the equation, which describes the fluorescence intensity of a particular fluorophore, the proportionality factor k appears [54]. This factor takes into account the experimental settings mentioned above. This value is generally unknown. Accordingly, the numerical value of the intensity has no meaning and it is expressed in arbitrary units.

5.3.13. Calorimetry

We performed the following three kinds of experiments to determine the thermodynamic parameters for the formation of complexes between the aggregates in IPW-HC and the base (aqueous NaOH):

i. Determination of the heat of dilution ΔH_{dil} ($m^i_x \rightarrow m^f_x$) from the initial molality (m^i) to the final molality (m^f) of binary aqueous solutions of NaOH, at the different concentrations employed.
ii. Determination of the heat of dilution ΔH_{dil} ($m^i_y \rightarrow m^f_y$) from the initial molality (m^i) to the final molality (m^f) of IPW-HC.
iii. Determination of the heat of mixing ΔH_{mix} [$(m^i_x)(m^i_y) \rightarrow m^f_x, m^f_y$] of IPW-HC with the binary aqueous NaOH solutions as probes.

We obtain the values of the experimental heats (of dilution or mixing) from the equation:

$$\Delta H = (dQ/dt)/P_w, \tag{1}$$

where dQ/dt/Watt is the heat flux and P_w/kg s^{-1} is the total mass flow-rate of the solvent through the calorimeter. ΔH is J kg^{-1} of solvent in the final solution. We used aqueous solutions of NaOH at different concentrations as probe solutions.

The heat of mixing we monitored by using a thermal activity monitor (TAM) model 2227, by Thermometric (Sweden) equipped with a flow mixing vessel. A P3 peristaltic pump (by Pharmacia) envoys the solutions into the calorimeter through Teflon tubes. The flow rates of the two liquids are the same. The rates are constant in the inlet tubes. Therefore, the solution coming out of the calorimeter has a concentration half the initial one. The mass flow-rate (constant within 1%) amounts to 3×10^{-3} g s^{-1}. It was the same for all the experiments.

We obtain the enthalpies of mixing the two solutions [IPW-HC and aqueous NaOH] by the following equations [31]:

$$\Delta H_{mix}\left[\left(m^i_x\right)\left(m^i_y\right) \rightarrow m^f_x, m^f_y\right] = \Delta H^* + \Delta H_{dil}\left(m^i_x \rightarrow m^f_x\right) + \Delta H_{dil}\left(m^i_y \rightarrow m^f_y\right). \tag{2}$$

The enthalpy of mixing of two binary solutions (ΔH_{mix}) is related to the enthalpy of formation of a complex, or in general to the enthalpy of interaction between solutes (ΔH^*) and to the heat of dilution experienced by the two solutes (ΔH_{dil}). IPW-HC, due to the practical absence of a solute, cannot produce any contribution to the heat of dilution and mixing via the y component. Consequently ΔH_{mix} [$(m^i_x)(m^i_y) \rightarrow m^f_x, m^f_y$] should coincide with ΔH_{dil} ($m^i_x \rightarrow m^f_x$) + ΔH^*, i.e., the dilution enthalpy of the probe plus an interaction term. We can express this interaction enthalpy (ΔH^*)as:

$$\Delta H^* = \Delta H^E, \tag{3}$$

where ΔH^E represents the excess enthalpy of mixing of the IPW-HC and the probe. ΔH^E is the contribution attributed to the presence of aggregates. The hypothesis is that some strong favourable interactions take place between the OH^- ions and the aggregates.

We assume that a complex of IPW-HC with NaOH forms. The following chemical equation represents the association process:

$$AG + nL = AGL_n, \tag{4}$$

where AG denotes the aggregates, n is the binding stoichiometry and L = OH^-. ΔH^E is normalized to the total molality (m_{AG}) of the aggregates. We obtain m_{AG} from the conductometric titration data. ΔH^E is a linear function of the actual molality of the titrant (m^f_L), of the standard molar enthalpy of association ($\Delta H°_a$), and of the apparent association constant (K'_a):

$$m_{AG}/\Delta H^E = 1/\Delta H°_a + 1/\left(\Delta H°_a K'_a m^f_L\right). \tag{5}$$

The actual concentration of the probe is given, for each value of ΔH^E, by:

$$m^f_L = m_L - \bar{x}\, m_{AG}, \tag{6}$$

where m_L is the total stoichiometric molality of the probe and $\bar{x}$ is the degree of binding.

For $\bar{x}$ holds:

$$x = \frac{1}{2 \cdot m_{AG}}\left(m_{AG} + n \cdot m_L + 1/K'_a\right) - \sqrt{\left(m_L + m_{AG} + 1/K'_a\right)^2 - 4 \cdot n \cdot m_L \cdot m_{AG}} \tag{7}$$

The standard molar enthalpy of association, the binding stoichiometry n and the apparent association constant are obtained from Eqs. (5), (6) and (7) by iterative least-squares fitting of the data. We fitted the data to a single set of identical binding sites models using ORIGIN 7.0 software. The iterations are continued until two successive values of Δ

$H°_a$ differ by <2%. The values for ΔH^E, $\Delta H^E/m_{AG}$ and m^f_{NaOH} are presented in Table S2.

The values of the free energy and entropy are computed from the usual thermodynamic relations. The absence of information about the activity coefficients leads to evaluations of the association parameters that are not precisely defined thermodynamically. We can only determine an apparent association constant K'_a. Consequently the standard free energy and entropy, respectively, $\Delta G°'_a$ and $\Delta S°'_a$, suffer from the same limitations. The thermodynamic parameters for the association are presented in Table S3.

Acknowledgments

We thank Dr. L. Elia for editing the manuscript. Tamar Yinnon thanks Prof. A.M. Yinnon for his support and proof reading of the manuscript.

Author contributions

V.E. conceived and managed the research. R.G. assisted in the latter task. E.N. prepared the perturbed water samples. R.O. measured the Circular Dichroism and Fluorescence spectra. G.P. carried out the MALDI-TOF/MS, GC/MS and gel electrophoresis measurements. E.N. performed the electric conductivity and pH measurements. D.T. carried out the optical microscopy measurements. G.V. provided the QFT explanations for some of the observed phenomena. L.L. and M.N. carried out the thermodynamic analyses. M.T. and A.G. carried out the IC analyses. T.A.Y. contributed to the theoretical analyses and wrote the manuscript. All authors discussed the results and commented on the manuscript.

Competing interests

The authors declare no competing financial interest.

Appendix A. Supplementary data

Supplementary data to this article can be found online at https://doi.org/10.1016/j.molliq.2018.07.045.

References

[1] D. Klemm, B. Heublein, H.P. Fink, A. Bohn, Cellulose: fascinating biopolymer and sustainable raw material, Angew. Chem. Int. Ed. 44 (2005) 3358–3393.
[2] V. Elia, N. Marchettini, E. Napoli, M. Niccoli, Calorimetric, conductometric and density measurements of iteratively filtered water using 450, 200, 100 and 25 nm Millipore filters, J. Therm. Anal. Calorim. 114 (2013) 927–936.
[3] V. Elia, G. Ausanio, A. De Ninno, R. Germano, E. Napoli, M. Niccoli, Experimental evidences of stable water nanostructures at standard pressure and temperature obtained by iterative filtration, Water 5 (2014) 121–130.
[4] A. Capolupo, E. Del Giudice, V. Elia, R. Germano, E. Napoli, M. Niccoli, A. Tedeschi, G. Vitiello, Self-similarity properties of Nafionized and filtered water and deformed coherent states, Int. J. Mod. Phys. B 28 (2014), 1450007. .
[5] (a) J.M. Zheng, W.C. Chin, E. Khijniak, E. Khijniak Jr., G.H. Pollack, Surfaces and interfacial water: evidence that hydrophilic surfaces have long-range impact, Adv. Colloid Interf. Sci. 127 (2006) 19–27;
(b) J.M. Zheng, G.H. Pollack, Solute exclusion and potential distribution near hydrophilic surfaces, in: G.H. Pollack, I.L. Cameron, D.N. Wheatley (Eds.), Water and the Cell, Springer, Netherlands, Dordrecht, 2006.
[6] B. Sulbarán, G. Toriz, G.G. Allan, G.H. Pollack, E. Delgado, The dynamic development of exclusion zones on cellulosic surfaces, Cellulose 21 (2014) 1143–1148.
[7] V. Elia, G. Ausanio, A. De Ninno, F. Gentile, R. Germano, E. Napoli, M. Niccoli, Experimental evidence of stable aggregates of water at room temperature and normal pressure after iterative contact with a Nafion® polymer membrane, Water 5 (2013) 16–26.
[8] V. Elia, E. Napoli, M. Niccoli, Physical–chemical study of water in contact with a hydrophilic polymer: Nafion, J. Therm. Anal. Calorim. 112 (2013) 937–944.
[9] V. Elia, L. Lista, E. Napoli, M. Niccoli, A thermodynamic characterization of aqueous nanostructures of water molecules formed by prolonged contact with the hydrophilic polymer Nafion, J. Therm. Anal. Calorim. 115 (2014) 1841–1849.
[10] V. Elia, R. Germano, E. Napoli, Permanent dissipative structures in water: the matrix of life? Experimental evidences and their quantum origin, Curr. Top. Med. Chem. 15 (2015) 559–571.
[11] V. Elia, T.A. Yinnon, R. Oliva, E. Napoli, R. Germano, F. Bobba, A. Amoresano, Chiral micron-sized H_2O aggregates in water: circular dichroism of supramolecular H_2O architectures created by perturbing pure water, Water 8 (2017) 1–29.
[12] T.A. Yinnon, V. Elia, E. Napoli, R. Germano, Z.-Q. Liu, Water ordering induced by interfaces: an experimental and theoretical study, Water 7 (2016) 96–128.
[13] N.F. Bunkin, P.S. Ignatiev, V.A. Kozlov, A.V. Shkirin, S.D. Zakharov, A.A. Zinchenko, Study of the phase states of water close to Nafion interface, Water 4 (2013) 129–154.
[14] Y. Zhang, S. Takizawa, J. Lohwacharin, Spontaneous particle separation and salt rejection by hydrophilic membranes, Water 7 (2015) 1–18.
[15] V. Elia, E. Napoli, Nanostructures of water molecules in iteratively filtered water, Key Eng. Mater. 495 (2011) 37–40.
[16] M. Laliberté, W.E. Cooper, Model for calculating the density of aqueous electrolyte solutions, J. Chem. Eng. Data 49 (2004) 1141–1151.
[17] J. Segarra-Martí, P.B. Coto, M. Rubio, D. Roca-Sanjuán, M. Merchán, Towards the understanding at the molecular level of the structured-water absorption and fluorescence spectra: a fingerprint of π-stacked water, Mol. Phys. 111 (2013) 1308–1315.
[18] B.-H. Chai, J.-M. Zheng, Q. Zhao, G.H. Pollack, Spectroscopic studies of solutes in aqueous solution, J. Phys. Chem. A 112 (2008) 2242–2247.
[19] S.-Y. Lo, Anomalous state of ice, Mod. Phys. Lett. 10 (1996) 909–919.
[20] A.I. Konovalov, I.S. Ryzhkina, Reviews: formation of nanoassociates as a key to understanding of physicochemical and biological properties of highly dilute aqueous solutions, Rus. Chem. Bull. Int. Ed. 63 (2014) 1–14.
[21] T.I. Quickenden, J.A. Irvin, The ultraviolet absorption spectrum of liquid water, J. Chem. Phys. 72 (1980) 4416–4428.
[22] P. Cabral do Couto, D.M. Chipman, Insights into the ultraviolet spectrum of liquid water from model calculations: the different roles of donor and acceptor hydrogen bonds in water pentamers, J. Chem. Phys. 137 (18430) (2012).
[23] J. Segarra-Martí, D. Roca-Sanjuán, M. Merchán, Can the hexagonal ice-like model render the spectroscopic fingerprints of structured water? Feedback from quantum-chemical computations, Entropy 16 (2014) 4101–4120.
[24] G.D. Fasman (Ed.), Circular Dichroism and the Conformational Analysis of Biomolecules, Springer Science+Business Media, New York, 1996.
[25] K.H. Ernst, Molecular chirality at surfaces, Phys. Status Solidi B 249 (2012) 2057–2088.
[26] M.L. McDermott, H. Vanselous, S.A. Corcelli, P.B. Petersen, DNA's chiral spine of hydration, ACS. Cent. Sci. 3 (2017) 708–714.
[27] V. Elia, T.A. Yinnon, R. Oliva, E. Napoli, R. Germano, F. Bobba, A. Amoresano, DNA and the chiral water superstructure, J. Mol. Liq. 248 (2017) 1028–1029.
[28] L.V. Belovolova, M.V. Glushkov, E.A. Vinogradov, V.A. Babintsev, V.I. Golovanov, Ultraviolet fluorescence of water and highly diluted aqueous media, Phys. Wave Phenom. 17 (2009) 21–31.
[29] E. Del Giudice, A. Tedeschi, G. Vitiello, V. Voeikov, Coherent structures in liquid water close to hydrophilic surfaces, J. Phys. Conf. Ser. 442 (2013), 012028. .
[30] A. De Ninno, Dynamics of formation of the exclusion zone near hydrophilic surfaces, Chem. Phys. Lett. 667 (2017) 322–326.
[31] V. Elia, M. Niccoli, Thermodynamics of extremely diluted aqueous solutions, Ann. N. Y. Acad. Sci. 879 (1999) 241–248.
[32] B. Chai, A.G. Mahtani, G.H. Pollack, Unexpected presence of solute-free zones at metal-water interfaces, Contemp. Mater. 3 (2012) 1–12.
[33] B. Chai, H. Yoo, G.H. Pollack, Effect of radiant energy on near-surface water, J. Phys. Chem. B 113 (2009) 13953–13958.
[34] V. Elia, M. Niccoli, New physico-chemical properties of extremely diluted aqueous solutions, J. Therm. Anal. Calorim. 75 (2004) 815–836.
[35] V. Elia, E. Napoli, M. Niccoli, L. Nonatelli, A. Ramaglia, E. Ventimiglia, New Physico-chemical properties of extremely diluted aqueous solutions. A calorimetric and conductivity study at 25 °C, J. Therm. Anal. Calorim. 78 (2004) 331–342.
[36] C.M. Cacace, L. Elia, V. Elia, E. Napoli, M. Niccoli, Conductometric and pH metric titrations of extremely diluted solutions using HCl solutions as titrant. A molecular model, J. Mol. Liq. 146 (2009) 122–126.
[37] T.A. Yinnon, V. Elia, Dynamics in perturbed very dilute aqueous solutions: theory and experimental evidence, Int. J. Mod. Phys. B 27 (2013) 1350005-1–1350005-35.
[38] I.S. Ryzhkina, S.Yu. Sergeeva, Y.V. Kiseleva, A.P. Timosheva, O.A. Salakhutdinova, M.D. Shevelev, A.I. Konovalov, Self-organization and properties of dispersed systems based on dilute aqueous solutions of (S)- and (R)-lysine, Mendeleev Commun. 28 (2018) 66–69.
[39] M. Blasone, P. Jizba, G. Vitiello, Quantum Field Theory and its Macroscopic Manifestations, Imperial College Press, London, 2011.
[40] G. Preparata, QED Coherence in Matter, World Scientific, Singapore, New Jersey, London, Hong Kong, 1995.
[41] R. Arani, I. Bono, E. Del Giudice, G. Preparata, QED coherence and the thermodynamics of water, Int. J. Mod. Phys. B 9 (1995) 1813–1841.
[42] I. Bono, E. Del Giudice, L. Gamberale, M. Henry, Emergence of the coherent structure of liquid water, Water 4 (2012) 510–532.
[43] E. Celghini, E. Graziano, G. Vitiello, Classical limit and spontaneous breakdown of symmetry as an environment effect of quantum field theory, Phys. Lett. A 145 (1990) 1–6.
[44] G. Vitiello, Coherent states, fractals and brain waves, New Math. Nat. Comput. 5 (2009) 245–264.
[45] G. Vitiello, Fractals and the Fock-Bargmann representation of coherent states, in: P. Bruza, D. Sofge, W. Lawless, K. van Rijsbergen, M. Klusch (Eds.), Quantum Interaction, Lecture Notes in Artificial Intelligence, Springer-Verlag, Berlin Heidelberg 2009, pp. 6–16.
[46] G. Vitiello, Fractals, coherent states and self-similarity induced noncommutative geometry, Phys. Lett. A 376 (2012) 2527–2532.

[47] G. Vitiello, in: J.R. Busemeyer, F. Dubois, A. Lambert-Mogiliansky, M. Melucci (Eds.), Fractals, Dissipation and Coherent States, in Quantum Interaction, 7620, Springer, Berlin, Heidelberg 2012, pp. 68–79.
[48] G. Vitiello, On the isomorphism between dissipative systems, fractal self-similarity and electrodynamics. Toward an integrated vision of nature, Systems 2 (2014) 203–216.
[49] T.A. Yinnon, Z.-Q. Liu, Domains formation mediated by electromagnetic fields in very dilute aqueous solutions: 2. Quantum electrodynamic analyses of experimental data on strong electrolyte solutions, Water 7 (2015) 48–69.
[50] T.A. Yinnon, Z.-Q. Liu, Domains formation mediated by electromagnetic fields in very dilute aqueous solutions: 3. Quantum electrodynamic analyses of experimental data on solutions of weak electrolytes and non-electrolytes, Water 7 (2015) 70–95.
[51] E.I. Klabunovskii, Homochirality and its significance for biosphere and the origin of life theory, Russ. J. Org. Chem. 48 (2012) 881–901.
[52] V.A. Pavlov, E.I. Klabunovskii, Homochirality origin in nature: possible versions, Curr. Org. Chem. 18 (2014) 93–114.
[53] Y. Scolnik, I. Portnaya, U. Cogan, S. Tal, R. Haimovitz, M. Fridkin, A.C. Elitzur, D.W. Deamer, M. Shinitzky, Subtle differences in structural transitions between poly-L- and poly-D-amino acids of equal length in water, Phys. Chem. Chem. Phys. 8 (2006) 333–339.
[54] B. Valeur, Molecular Fluorescence: Principles and Applications, Wiley-VCH, 2002.